



Influence of the oxidation behavior of Ti–6Al–4V alloy in dry air on the oxide layer microstructure

Lamiaa Z. Mohamed¹ · S. S. Abd Elmomen² · Shima El-Hadad³

Received: 3 August 2021 / Accepted: 5 November 2021 / Published online: 3 January 2022
© Institute of Chemistry, Slovak Academy of Sciences 2021

Abstract

The effects of isothermal oxidation parameters on the oxidation kinetics and morphology of the oxides layers obtained on Ti–6Al–4V alloy (Ti64) at 650, 750 and 850 °C for 50 h in dry air were studied. Morphology of the oxide scales was examined by scanning electron microscopy (SEM) and the energy-dispersive X-ray analysis (EDX). The phases in the scales were characterized by X-ray diffraction. The rate of oxidation at the different temperatures was described by a parabolic equation, and the oxidation activation energy value was 191.7 kJ/mol. The parabolic rate constants were 8.80×10^{-9} , 7.48×10^{-8} and 7.68×10^{-7} g²/(cm⁴.h) at 650 °C, 750 °C and 850 °C, respectively. The morphologies through the cross section of the oxide layers were analyzed by SEM, spot and line EDX. The analysis of the oxide scale revealed mainly TiO₂ and small amount of Al₂O₃. The oxide layers were discontinuous and non-protective layers at 750 °C and 850 °C.

Keywords High-temperature oxidation · Ti–6Al–4 V alloy · Microstructure · Activation energy

Introduction

The maximum service temperature of Ti–6Al–4V (Ti64) is limited partly because of the growth of an oxide layer at temperatures above 480 °C and the concurrent transition of the oxide to more active, non-protective state (Brice et al. 2016; Fargas et al. 2017). Also, to keep its mechanical stability which plays a key role on the behavior of Ti64 for different applications. The oxide scale is protective during the early stage of oxidation, but after a lengthy period of oxidation, it loses its protective scale and increases the oxygen diffusion through the oxide (Fargas et al. 2017). The Ti64 accounts for nearly 60% of the produced Ti-alloys and uses in a wide range of applications (Brice et al. 2016). Ti64 alloy has a two-phase structure ($\alpha + \beta$) which contains 6%Al (α -hcp phase stabilizer) and 4%V (β -BCC phase stabilizer) (Mungole et al. 2002; Dong et al. 2017a; Oh et al. 2017;

Abdel-Salam et al. 2019; Abe et al. 2020). Airframes, aero gas turbine engines and compressors, pressure containers, gas and chemical pumps, cryogenic parts, and marine components, as well as high- and low-pressure steam turbine blades, are examples of Ti64 alloy applications (Dong et al. 1997; Li et al. 2017; Caballero et al. 2019; Dai et al. 2018; Valdés-Saucedo et al. 2021; Nesli et al. 2021). However, oxidation is still the central problem that limited wider applications of these alloys. Oxygen and nitrogen are strong alpha stabilizers in Ti64 alloys. Oxygen enriched hard layer of alpha phase is generated beneath the surface by the oxidation process. The depth of alpha case layer in Ti64 ingots may reach up to 250 μ m. Formation of this alpha case is a serious metallurgical problem (Kazantseva et al. 2017). Although Ti has a high corrosion resistance at room temperature, this is not the case when exposed to high temperatures due to the formation of thin and passive TiO₂ protective scale (Ma et al. 2020). The TiO₂ scale, which has been shown to be highly permeable to oxygen, loses its protective characteristics at temperatures above 500 °C, allowing oxygen to penetrate into the bulk metal. This diffused oxygen acts as a stabilizer of the alpha phase (Caballero et al. 2019; Dai et al. 2018).

The natively formed oxide layer exhibits a non-uniform oxygen concentration throughout the thickness which consider a serious problem. The oxide scale first forms and then grows and starts to crack upon exposure

✉ Lamiaa Z. Mohamed
lamiaa.zaky@cu.edu.eg

¹ Mining, Petroleum, and Metallurgical Engineering Department, Faculty of Engineering, Cairo University, Giza, Egypt

² Tabbin Institute for Metallurgical Studies, Helwan, Egypt

³ Central Metallurgical Research and Development Institute (CMRDI), P.O. 87, Helwan, Egypt

to compressive stress and ends by a material failure. As a result of thick oxide scales formation, the service temperature of most commercially available Ti alloys has a significant limiting factor (Brice et al. 2016). Additionally, it is known that oxygen has high solid solubility in α -titanium (about 14.5 wt.%). Therefore, exposure of Ti64 to temperatures above 480 °C in an oxygen containing environment results in simultaneous formation of an oxide scale, which consists of a multilayered structure of TiO_2 and Al_2O_3 , and the oxygen enriched layer beneath this scale (Fargas et al. 2017).

Although various investigations into the oxidation behavior of Ti64 from an application viewpoint have been undertaken, there have been few attempts to correlate the oxidation mechanism at temperatures above 850 °C (Dong et al. 2017a, b; Casadebaigt et al. 2020). A multilayered oxide scale with alternating layers of Al_2O_3 and TiO_2 formed on Ti64 upon oxidation in air at 750 °C. Another study examined the oxidation behavior in air of Ti64 at 600–700 °C and found that the onset of the duplex nature began at 650 °C and became more pronounced as time and temperature went on (Dong et al. 2017a). The activation energy was calculated as 88 kJ/mol in the temperature range of 777–1077 °C (Mungole et al. 2002). In the temperature range of 600–800 °C, the activation energy values were 276 kJ/mole and 191 kJ/mole for the parabolic and linear oxidation stages, respectively (Kazantseva et al. 2017). In another research, the activation energy of Ti64 in dry air in the temperature range of 850–1000 °C was 147 kJ/mol (Bandeira et al. 2020).

In the production of Ti alloys, oxides can have both positive and negative effects on the performance properties of Ti product. Surface oxidation is carried out to improve wear resistance, erosion resistance, fatigue resistance, and corrosion resistance. The solution of technological problems associated with oxidation process is urgent. Thus, the research carried out in this work is devoted to a topical scientific problem in order to provide reasonable process parameters for improving the oxidation resistances of Ti64 alloy at 650, 750 and 850 °C in dry air for 50 h. The activation energy was estimated in the investigated temperature range. The surface morphology and analysis of the cross section of the oxide layer were also studied at the investigated temperatures. The constituting phases of the oxide layer were investigated. The obtained results are expected to provide the necessary process parameters to minimize the negative effects of oxidizing the large-sized Ti ingots.

Experimental work

Material

Forged bars of Ti64 alloy were received from BAOJI XUHE Titanium Metal Co., LTD. These bars were processed by melting in 500 kg vacuum induction furnace to obtain billets with the chemical composition shown in Table 1, followed by forging and machining into 10-mm-diameter rods.

Prior to oxidation, samples of 1 cm thickness and 1 cm diameter were ground by emery papers from grit size 100–1000 and then polished by alumina paste 0.3 μm . The etching solution used for investigated alloy was 7% HF, 8% HNO_3 , and the rest was distilled water. The morphology of the samples was observed by SEM (FEI inspect S-Netherlands) and EDX (Bruker AXS-flash detector Germany).

Oxidation

The oxidation process was carried out at temperatures of 650, 750 and 850 °C for duration that ranged between 5 and 50 h in dry air at a rate of 2 lit/min. A vertical tube furnace (model EVA 12/300B- CARBOLITE GERO) was used for this purpose. A computer program “version programmer 3216 P5” was used to control the oxidation process. Mass changes of the samples were monitored along the oxidation period at time intervals of 5 h by a high accuracy electrical balance (METTLER—TOLEDO Model MS 204 S/01).

The phases of the oxide layer were investigated by X-ray diffractometer analyzer, model (X’Pert PRO PAN analytical diffractometer) with Cu $K\alpha$ radiation source $\lambda = 0.15406$ nm, 45 kV and 40 mA. The detector was moving through an angle from 10 to 100°. The oxidized samples were studied by line EDX to demonstrate the elemental distribution across the oxide layer at 50 h for the investigated temperatures.

Results and discussions

Alloy microstructure

Figure 1 and Table 2 show the SEM microstructure and EDX of forged Ti64 alloy before oxidation. The microstructure constituents are two phases (α and β) as shown in Fig. 1. The dark regions in Fig. 1c present the primary α phase, while the thin bright regions are β phase that exists between α plates. It was reported that the elemental Al and V diffuse into α and β

Table 1 The chemical composition of as-received Ti64 alloy

Elements, wt. %	Al	V	Fe	O	C	N	Nb	Others	Ti
Ti64	6.1	4	0.1	0.03	0.02	0.01	0.01	<0.4	Bal.

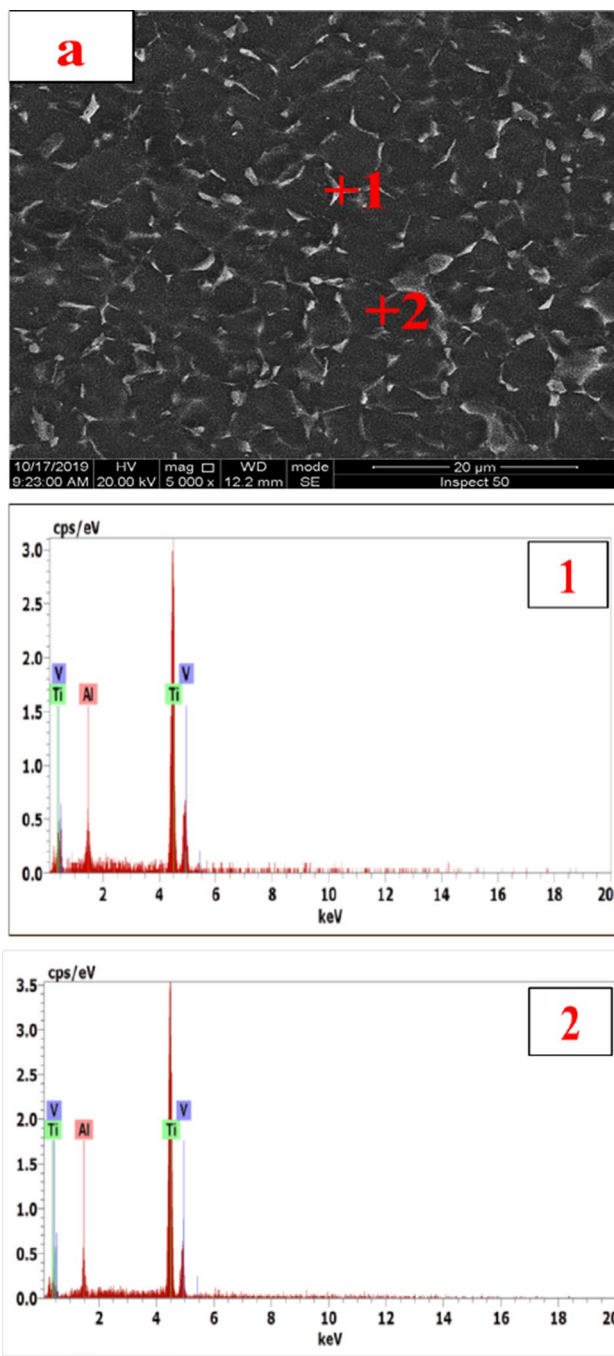


Fig. 1 SEM microstructure and EDX patterns of the forged Ti64 before oxidation

Table 2 Spot EDX analysis of the alloy before oxidation

Spot no.	Elements, wt. %		
	Al	V	Ti
Spot 1	5.19	4.68	Bal.
Spot 2	5.63	0.57	Bal.

phases, respectively, during cooling (Oh et al. 2017; Bandeira et al. 2020).

Oxidation kinetics

Figure 2 provides the weight gain per unit area vs. oxidation time for Ti64 at 650 °C, 750 °C and 850 °C. The weight gain curves in Fig. 2 show that the examined alloy has noticed to give different oxidation behaviors at different temperatures and times. At temperature 650 °C, the weight change per unit area was stable and slowly increases with increasing time. At temperature 750 °C, a slight increase in the weight gain up to 20 h can be detected and then the weight change was relatively stable with increasing time. However, at 850 °C the weight gain increased remarkably with time. In general, the high-temperature oxidation kinetics can be described by Eq. (1):

$$(\Delta W/\Delta A)^n = K_p t \quad (1)$$

where ΔW is the weight gain per unit area, K_p is the rate constant and t is the oxidation time, and n is the rate exponent. The value of n is approximately 2, so the oxidation kinetics of Ti64 is parabolic. The oxidation rate constant k_p can be determined by plotting $(\Delta W/A)^2$ against t , and the results are displayed in Table 3.

The activation energy of Ti64 alloy could be obtained by drawing $\log K_p$ against $1/T$ as shown in Fig. 3. According to the Arrhenius equation, the straight line satisfies the formula in Eq. (2) (Casadebaigt et al. 2018).

$$K_p = K_p e^{(-Q/RT)} \quad (2)$$

Therefore, the activation energy of the oxidation of Ti64 alloy in the temperature range between 650 and 850 °C for 50 h in dry air is 191.7 kJ/mole which compares with 191 and 192 kJ/mol found elsewhere for the oxidation reaction (Aniołek et al. 2015; Guleryuz et al. 2009).

Fig. 2 The variation of weight gain ($\Delta W/A$) against the oxidation time of Ti64 alloy at 650 °C, 750 °C and 850 °C in dry air for 50 h

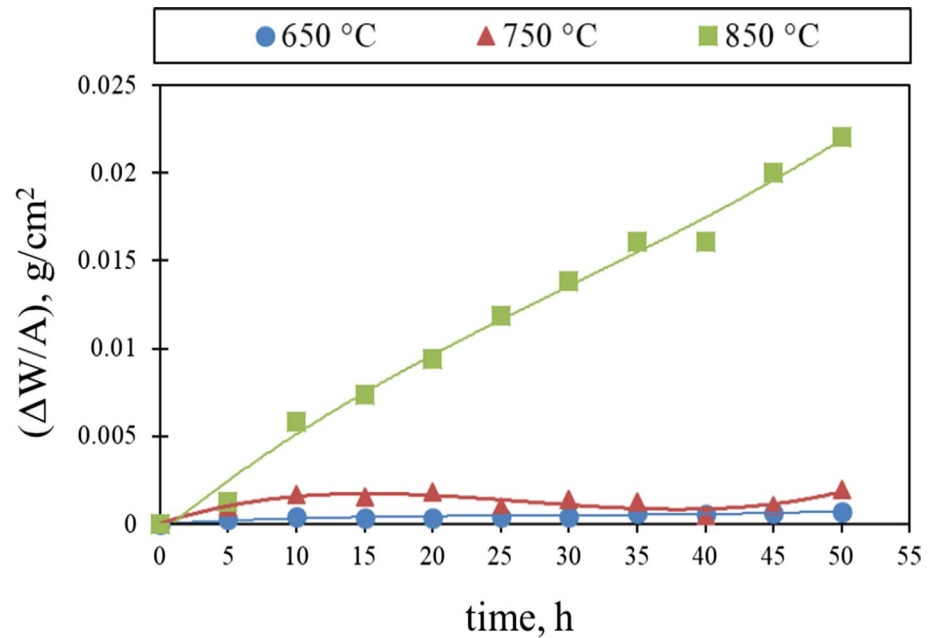


Table 3 The rate constant k_p of Ti64 alloy oxidized at 650 °C, 750 °C and 850 °C

Temperature °C	650 °C	750 °C	850 °C
k_p , g ² cm ⁻⁴ h ⁻¹	8.80×10^{-9}	7.48×10^{-8}	7.68×10^{-7}

of TiO₂ and Al₂O₃. Peaks of Ti- α phase are visible due to the thin thickness of the oxide layer. There are no peaks for titanium nitrides due to lower content or lower crystallinity.

Surface morphology after oxidation

Surface morphology at 650 °C

The surface morphologies and EDX results of the oxide layer are given in Fig. 5 at 5 h, 25 h and 50 h for 650 °C. It can be observed that the surfaces are crack-free with uniform roughness, which increases with the increase in oxidation

Phase identifications

The X-ray diffraction patterns of the oxidized specimens at 650 °C, 750 °C and 850 °C for 50 h are given in Fig. 4. The oxidized surfaces of the Ti64 alloy principally consist

Fig. 3 The Arrhenius plot of the parabolic rate constant for the oxidation of Ti64 alloy in the temperature range of 650–850 °C for oxidation times of up to 50 h in dry air

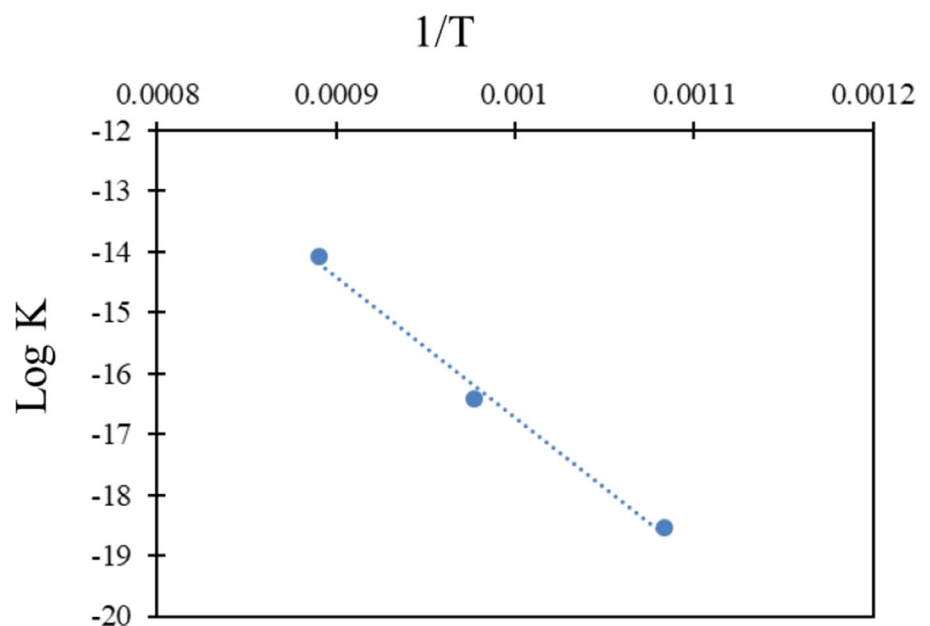
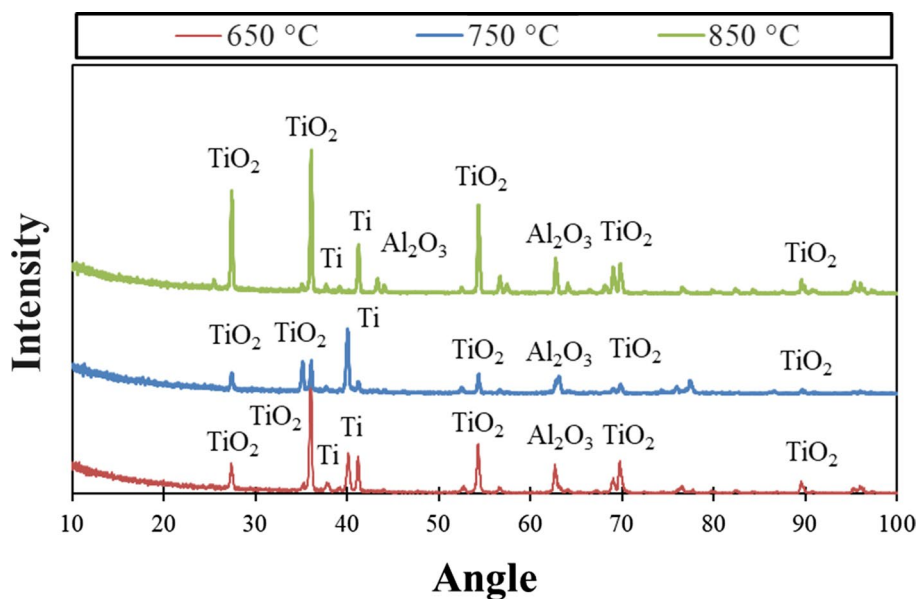


Fig. 4 The XRD patterns of the outer oxide surfaces of Ti64 at 650 °C, 750 °C and 850 °C for 50 h in dry air



temperature. The EDX analysis for Spots 3, 4 and 5 is tabulated in Table 4. It can be noted that increasing the time thickens the oxide layer by increasing the oxygen content. Figure 6 shows the SEM morphology of the cross section of the oxide layer at 650 °C and the elemental distribution by line EDX through it. In the outside layer, O, Al and Ti increase thus forming Al_2O_3 and TiO_2 , while V increases at the oxide/alloy interface as provided from Fig. 6. Nitrogen appears in some areas at 50 h as listed in Table 4 which might be due to the formation of titanium nitrides; also the intensity of O and Al increased compared to at 25 h and V is almost the same. Spot 6 was at the air/oxide interface, while Spot 7 at the oxide/alloy interface, and their analysis is listed in Table 5. Oxide layers with significantly higher thickness are obtained at 650 °C for 50 h. The average thickness of the oxide layer for a forged Ti64 isothermally oxidized at 650 °C for 50 h was about 7 μm .

Surface morphology at 750 °C

The surface morphologies and spot EDX of the oxidized Ti64 at 750 °C for 5 h, 25 h and 50 h are given in Fig. 7, and the corresponding EDX analysis of Spots 8, 9 and 10 is listed in Table 6. Nitrogen appears also after 50 h in a relatively higher content than at 650 °C, which may be due to formation of titanium nitrides which accomplished with a decrease

in O, Al and V content than at 25 h. The elemental distribution across the oxide layer is shown in Fig. 8, and Spots 11 and 12 are illustrated in Table 7. It is clear that the oxide layers are separated at the oxide/alloy surface as shown in Fig. 8 and start to contain a new layer of the oxides. The separated oxide layers were about 20 μm , while the new layer was around 2 μm at 850 °C and 50 h as shown in Fig. 8b.

Surface morphology at 850 °C

The surface morphologies and spot EDX analysis of the oxidized Ti64 at 850 °C for 5 h, 25 h and 50 h are presented in Fig. 9. The EDX results for Spots 13, 14 and 15 are listed in Table 8. Nitrogen at 50 h appears with a lower decrease in O, Al and V than at 25 h for 850 °C. This might be due to the formation of a titanium nitrides. The elemental distribution across the oxide layer is given in Fig. 10, and spot EDX results of Spots 16 and 17 are illustrated in Table 9. The oxide layers were separated at the oxide/alloy surface as shown in Fig. 10 and began to contain a new layer of the oxides. The phenomena of non-uniform oxide layer coverage may be related to the layer growth process, which includes the development of thin oxide scale in the first stage, followed by its aggregation and expansion, and finally the formation of an oxide layer on the entire surface (Aniołek et al. 2018). Oxide layers with significantly higher thickness were

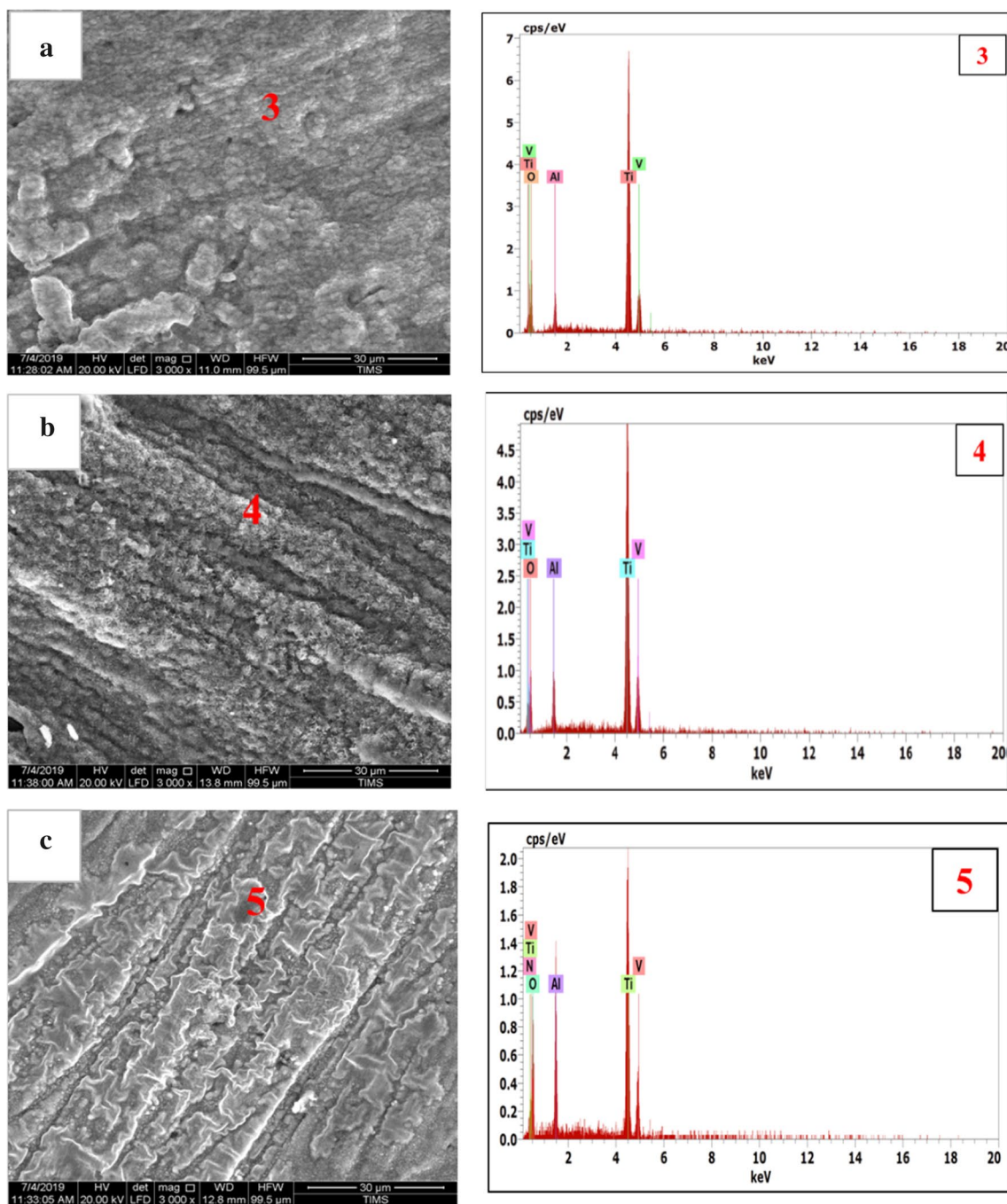
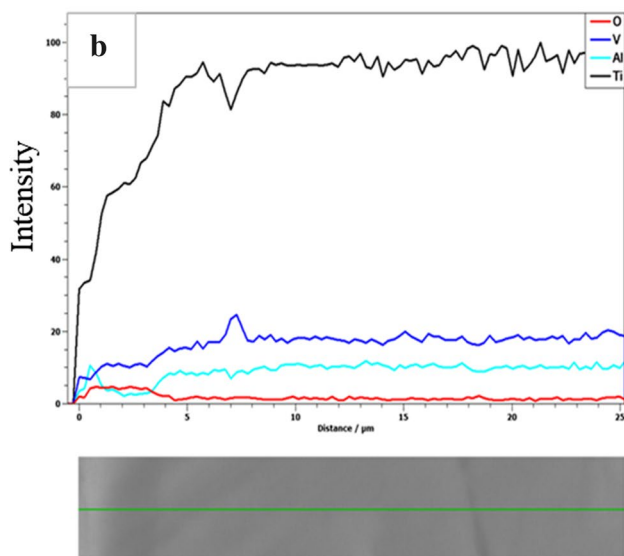
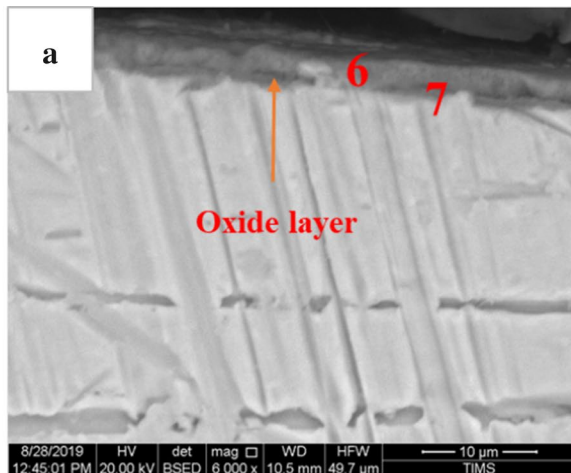


Fig. 5 The SEM morphologies of Ti64 alloy at 650 °C in dry air for a 5 h, b 25 h and 50 h

Table 4 Spot EDX analysis of the surface oxide layer at 650 °C

Time, h	Spot no.	Elements, wt.%				
		O	N	Al	V	Ti
5	Spot 3	36.2	0	3.3	1.1	Bal.
25	Spot 4	35.3	0	4.3	2.1	Bal.
50	Spot 5	45.9	3.4	7.6	2.0	Bal.

**Fig. 6** The cross section of oxide layer at 650 °C for 50 h in dry air **a** SEM and **b** line EDX**Table 5** Spot EDX analysis of the cross section of the oxide layer for 50 h at 650 °C

Spot no.	Elements, wt.%			
	O	Al	V	Ti
Spot 6	40.6	10.7	1.4	Bal.
Spot 7	15.5	2.5	3.5	Bal.

obtained at 850 °C for 50 h. The average thickness of a separated oxide layer for a forged Ti64 isothermally oxidized at 850 °C for 50 h was 120 μm, while the new layer is about 10 μm. Increasing the oxidation temperature increased the oxidation rate.

General discussion

The XRD patterns identify the existence of TiO₂ and Al₂O₃ in all the investigated oxidation temperatures as shown in Fig. 4 which also shows the existence of Ti peaks from the Ti64 alloy. This is confirmed from EDX patterns from the surface morphologies and cross section elemental line EDX for 650 °C, 750 °C and 850 °C. At 650 °C, the growth of the oxide layer from 5 to 50 h all over the alloy surface is shown in Figs. 5 and 6 with about 7 μm oxide thickness. It is notable that XRD patterns did not show titanium nitrides due to their low content. Increasing the Al element peak intensity from Spots 3 to 5 increases the oxidation time. However, for 750 °C and 850 °C, the oxide layer was completely separated and began to grow another one as shown from Figs. 7, 8, 9 and 10. The Al element intensity of the peak was almost equal for 5 h and 25 h and decreased for 50 h for 750 °C in Fig. 7. This may be due to the separation of the oxide layers after 25 h. At 850 °C, multilayers

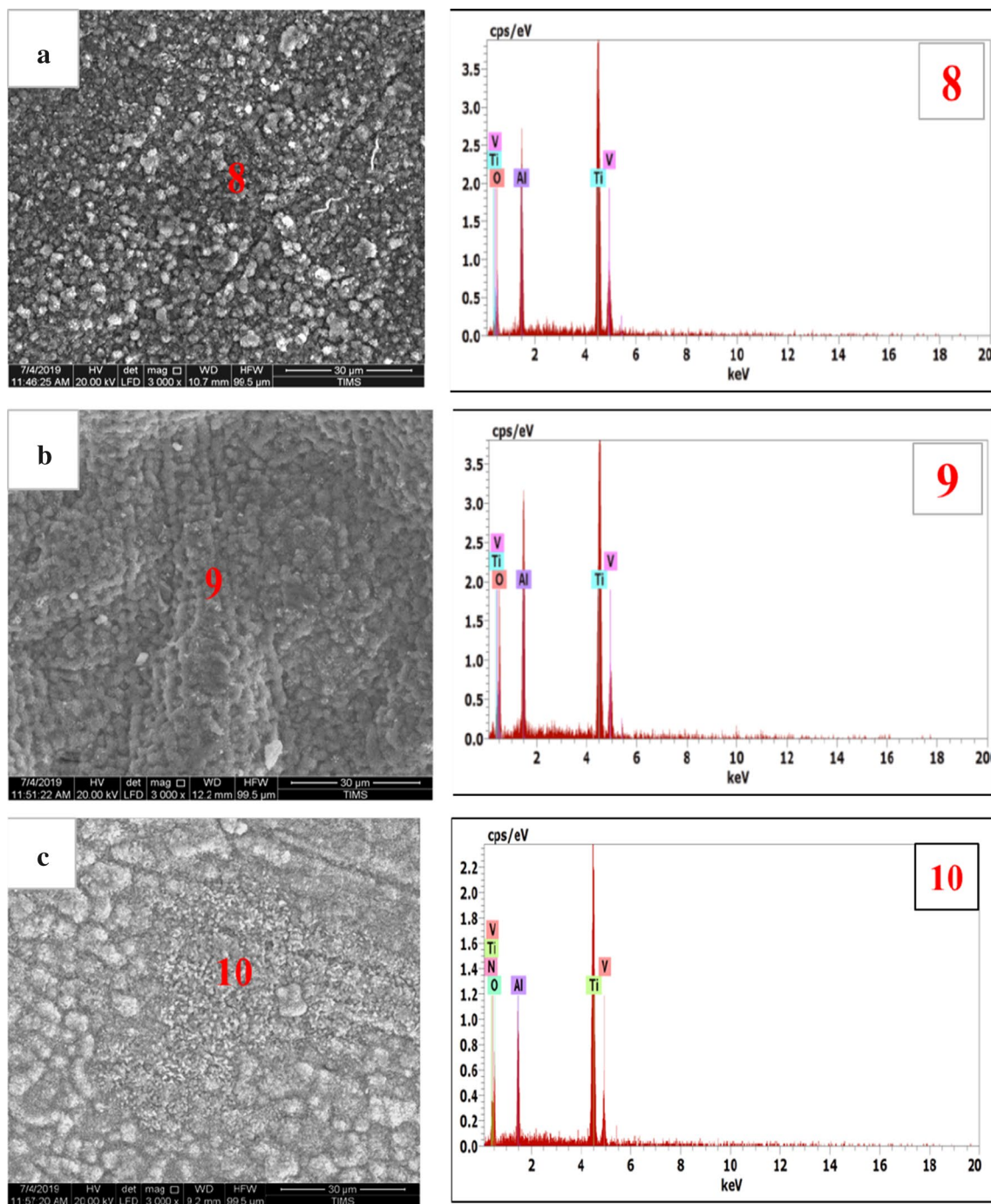


Fig. 7 The oxide surfaces at 750 °C for **a** 5 h, **b** 25 h and 50 h

Table 6 Spot EDX analysis of the surface oxide layer for 5 h at 750 °C

Time, h	Spot no.	Elements, wt. %				
		O	N	Al	V	Ti
5	Spot 8	32.8	0	13.1	3.1	Bal.
25	Spot 9	42.1	0	11.1	3.1	Bal.
50	Spot 10	36.4	8.0	7.1	0.6	Bal.

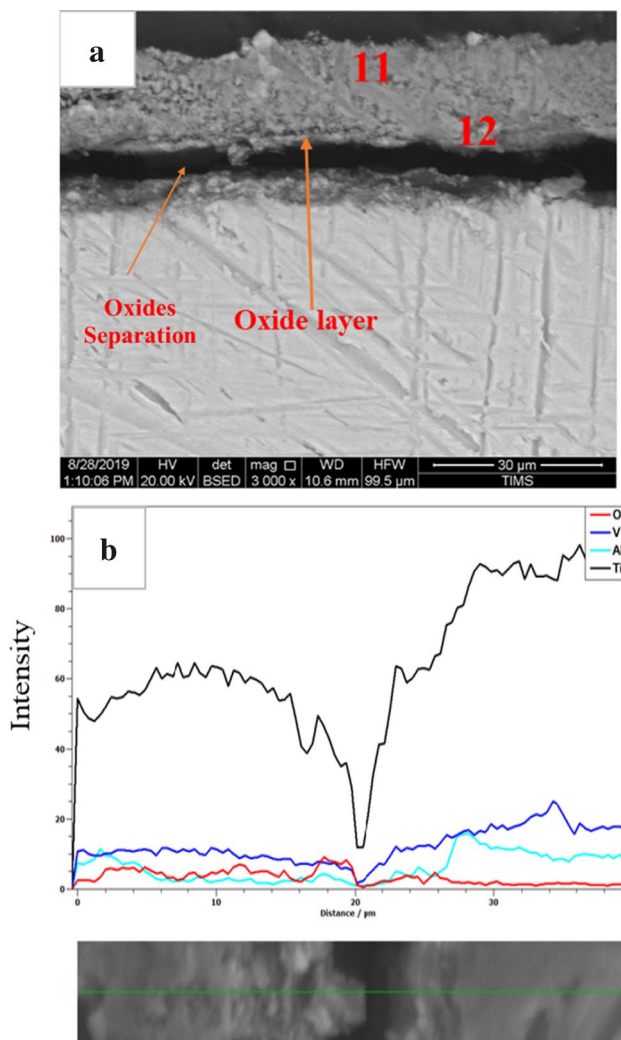


Fig. 8 The cross section of the oxide layer at 750 °C for 50 h **a** SEM and **b** line EDX

Table 7 Spot EDX analysis of the cross section of the oxide layer for 50 h at 750 °C

Spot no.	Elements, wt. %			
	O	Al	V	Ti
Spot 11	35.4	10.2	2.8	Bal.
Spot 12	10.8	10.1	3.9	Bal.

with cracks are presented in Fig. 10. The intensity of Al element peaks from EDX pattern decreases at 25 h which might be due to the separation of the oxide layers before 25 h and began to increase again at 50 h, as given in Fig. 9. The oxidation layer at 850 °C is thicker than the others. The main important effect on the oxidation stability is the oxygen diffusion because it stabilized the alpha phase (Valdés-Saucedo et al. 2021). In all the investigated oxidation temperatures, Al⁺ ions went to the surface and contain Al₂O₃ as clusters not as continuous layers proved by SEM morphologies, spot and line EDX.

Conclusion

The isothermal oxidation of forged Ti64 alloy was investigated at 650 °C, 750 °C and 850 °C for 50 h in dry air. The parabolic rate constants were 8.80×10^{-9} , 7.48×10^{-8} and $7.68 \times 10^{-7} \text{ g}^2/(\text{cm}^4 \cdot \text{h})$ at 650 °C, 750 °C and 850 °C, respectively. The obtained oxidation activation energy value was 191.7 kJ/mol. The phases present in the scales were complex and composed mainly of TiO₂ and Al₂O₃. The continuity of the scale and the size of oxide particles were decreasing with temperature. The oxide layers are discontinuous and non-protective layers at 750 °C and 850 °C.

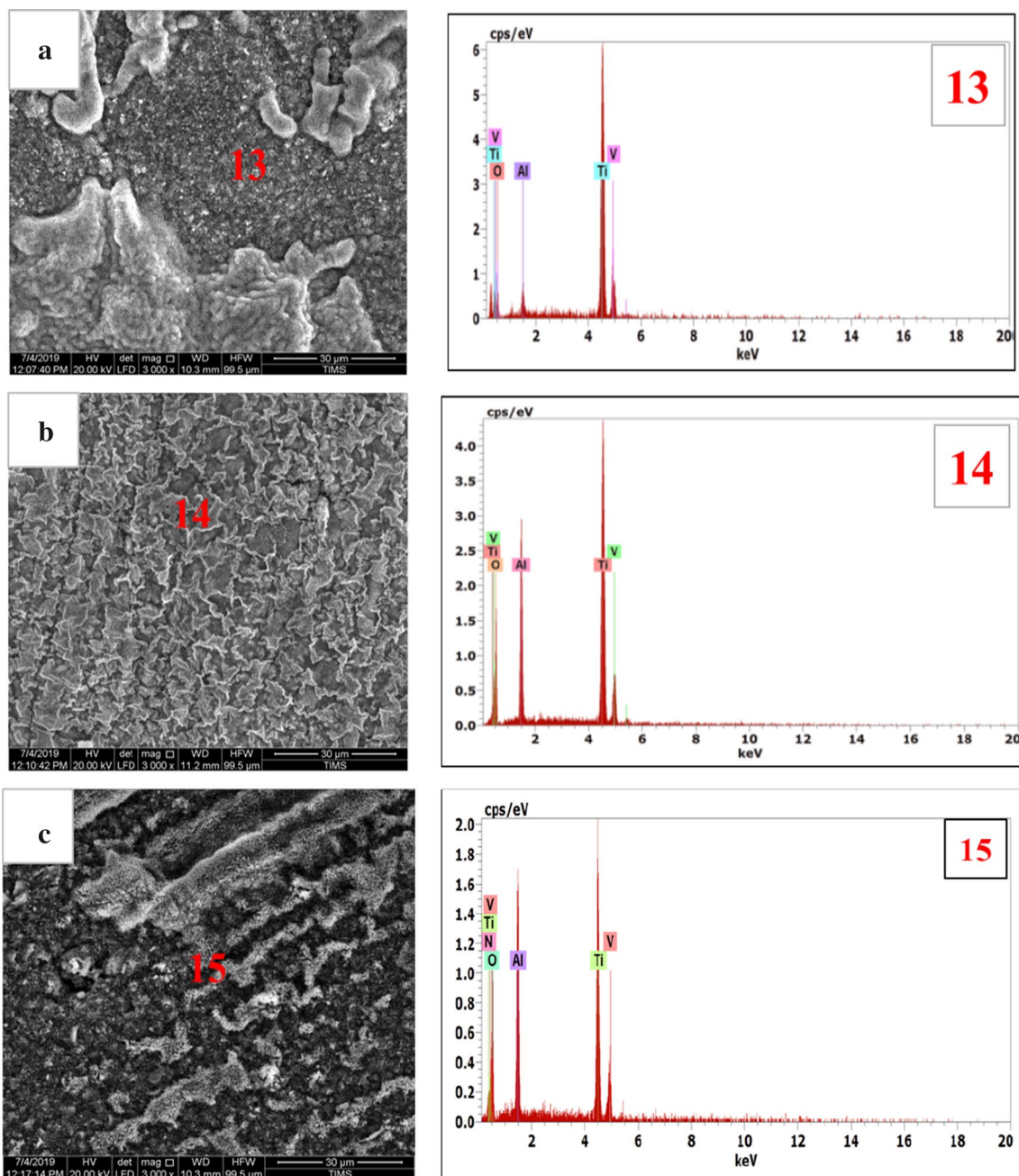


Fig. 9 The oxide surfaces at 850 °C for **a** 5 h, **b** 25 h and 50 h

Table 8 Spot EDX analysis of the surface oxide layer at 850 °C

Time, h	Spot no.	Elements, wt.%				
		O	N	Al	V	Ti
5	Spot 13	24.7	0	2.9	2.3	Bal.
25	Spot 14	48.8	0	13.1	2.1	Bal.
50	Spot 15	43.6	4.9	10.7	1.1	Bal.

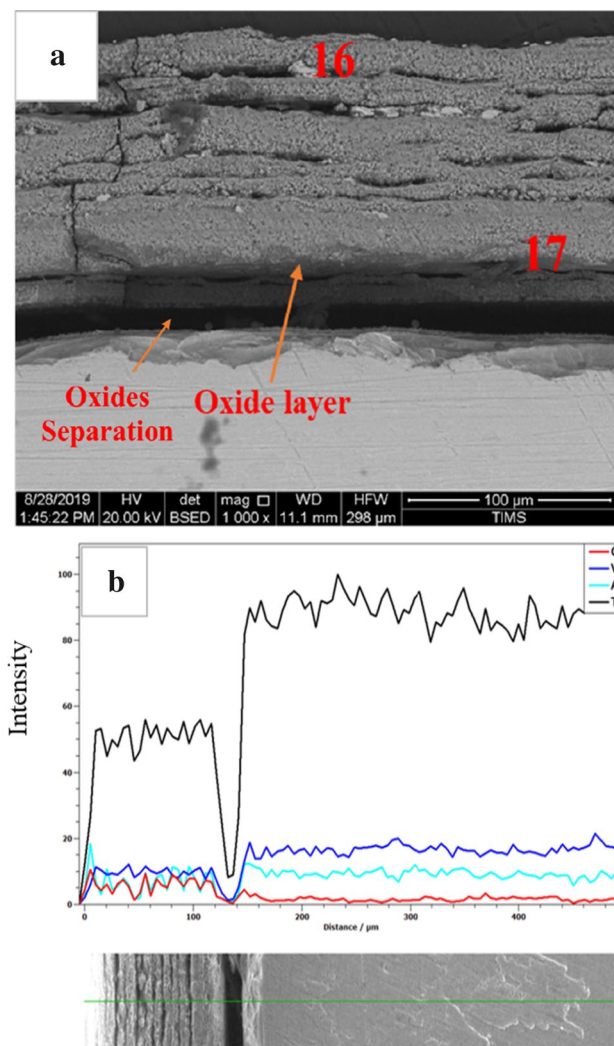


Fig. 10 The cross section of the oxide layer at 850 °C for 50 h **a** SEM and **b** line EDX

Table 9 Spot EDX analysis of the cross section of the oxide layer for 50 h at 850 °C

Spot no.	Elements, wt.%			
	O	Al	V	Ti
Spot 16	41.5	1.9	1.9	Bal.
Spot 17	1.9	6.0	2.5	Bal.

Declarations

Conflict of interest There are no conflicts of interest to declare.

References

Abdel-Salam M, El-Hadad S, Khalifaa W (2019) Effects of microstructure and alloy composition on hydroxyapatite precipitation on alkaline treated α/β titanium alloys. *Mater Sci Eng C* 104:109974

- Abe JO, Popoola API, Popoola OM (2020) Consolidation of Ti6Al4V alloy and refractory nitride nanoparticles by spark plasma sintering method: microstructure, mechanical, corrosion and oxidation characteristics. *Mater Sci Eng A* 774:138920
- Aniołek K, Kupka M, Łuczuk M, Barylski A (2015) Isothermal oxidation of Ti–6Al–7Nb alloy. *Vacuum* 114:114–118
- Aniołek K, Barylski A, Kupka M (2018) Modelling the structure and mechanical properties of oxide layers obtained on biomedical Ti–6Al–7Nb alloy in the thermal oxidation process. *Vacuum* 154:309–314
- Bandeira RM, Rêgo GC, Picone CA, Drunen JV, Correr WR, Casteletti LC, Machado SAS, Tremiliosi-Filho G (2020) Alternating current oxidation of Ti–6Al–4V alloy in oxalic acid for corrosion resistant surface finishing. *SN Appl Sci* 2:1092
- Brice DA, Samimi P, Ghamarian I, Liu Y, Brice RM, Reidy RF, Cotton JD, Kaufman MJ, Collins PC (2016) Oxidation behavior and microstructural decomposition of Ti–6Al–4V and Ti–6Al–4V–1B sheet. *Corros Sci* 112:338–346
- Caballero A, Ding J, Bandari Y, Williams S (2019) Oxidation of Ti–6Al–4V during wire and arc additive manufacture. *3D Print Addit Manuf.* <https://doi.org/10.1089/3dp.2017.0144>
- Casadebaigt A, Hugues J, Monceau D (2018) Influence of microstructure and surface roughness on oxidation kinetics at 500–600 °C of Ti–6Al–4V alloy fabricated by additive manufacturing. *Oxid Met* 90(5–6):633
- Casadebaigt A, Monceau D, Hugues J (2020) High temperature oxidation of Ti–6Al–4V alloy fabricated by additive manufacturing influence on mechanical properties. In: *The 14th world conference on titanium, MATEC Web of Conferences vol 321*, p 03006
- Dai J, Zhang N, Wang A, Zhang H, Chen C (2018) Microstructure and high temperature oxidation behavior of Ti–Al–Nb–Si coatings on Ti–6Al–4V alloy. *J Alloy Compd* 765:46–57
- Dong H, Bloyce A, Morton PH, Bell T (1997) Surface engineering to improve tribological performance of Ti–6Al–4V. *Surf Eng* 13(5):402–406
- Dong E, Yu W, Cai Q, Cheng L, Shi J (2017a) High temperature oxidation kinetics and behavior of Ti–6Al–4V alloy. *Oxid Met* 88:719–732
- Dong E, Yu W, Cai Q (2017b) Alpha-case kinetics and high temperature plasticity of Ti–6Al–4V alloy oxidized in different phase regions. *Procedia Eng* 207:2149–2154
- Fargas G, Roa JJ, Sefer B, Pederson R, Antti ML, Mateo A (2017) Oxidation behavior of Ti–6Al–4V alloy exposed to isothermal and cyclic thermal treatments. *Metal*
- Guleryuz H, Cimenoglu H (2009) Oxidation of Ti–6Al–4V alloy. *J Alloys Compd* 472:241–246
- Kazantseva N, Krakhmalev P, Yadroitsev I, Fefelov A, Merkushev A, Ilyinikh M, Vinogradova N, Ezhov I, Kurennykh T (2017) Effect of oxygen and nitrogen contents on the structure of the Ti–6Al–4V alloy manufactured by selective laser melting. In: *Scientific proceedings III international scientific conference "Material science nonequilibrium phase transformations" YEAR I*, 5–7
- Li G, Ren Z, Qu S, Li X (2017) Surface modification layer of Ti–6Al–4V produced by surface rolling and thermal oxidation. *Innovations* 5(4):232–242
- Ma K, Zhang R, Sun J, Liu C (2020) Oxidation mechanism of biomedical titanium alloy surface and experiment. *Int J Corros* 8:1–9
- Mungole MN, Singh N, Mathur GN (2002) Oxidation behaviour of Ti6Al4V titanium alloy in oxygen. *Mater Sci Technol* 18(1):111–114
- Nesli S, Yilmaz O (2021) Surface characteristics of laser polished Ti–6Al–4V parts produced by electron beam melting additive manufacturing process. *Int J Adv Manuf Technol* 114:271–289
- Oh ST, Woo KD, Kim JH, Kwak SM (2017) The effect of Al and V on microstructure and transformation of β phase during

solution treatments of cast Ti–6Al–4V alloy. *Korean J Met Mater* 55(3):150–155

Valdés-Saucedo OA, Rocha-Moreno RC, Ramírez-Ramírez JH, Pérez-González FA, Colás R, Garza-Montes-de-Oca NF (2021) Characterization of the high temperature isothermal oxidation behaviour

of an ATI425® titanium alloy. *Oxid Met.* <https://doi.org/10.1007/s11085-021-10032-z>

Publisher's Note Springer Nature remains neutral with regard to jurisdictional claims in published maps and institutional affiliations.